

See discussions, stats, and author profiles for this publication at: <https://www.researchgate.net/publication/231232947>

Uniform α -Fe₂O₃ Nanocrystal Moniliforme-Shape Straight-Chains

ARTICLE *in* CRYSTAL GROWTH & DESIGN · DECEMBER 2009

Impact Factor: 4.89 · DOI: 10.1021/cg901116c

CITATIONS

34

READS

44

6 AUTHORS, INCLUDING:



[Chinping Chen](#)

Peking University

97 PUBLICATIONS 1,667 CITATIONS

[SEE PROFILE](#)



[Heping Zhou](#)

Tsinghua University

105 PUBLICATIONS 1,165 CITATIONS

[SEE PROFILE](#)



[Yadong Li](#)

Tsinghua University

355 PUBLICATIONS 24,355 CITATIONS

[SEE PROFILE](#)

Uniform α -Fe₂O₃ Nanocrystal Moniliforme-Shape Straight-Chains

L-r Meng,[†] Weimeng Chen,[‡] Chinping Chen,[‡] Heping Zhou,[†] Qing Peng,[†] and Yadong Li^{*,†}

[†]State Key Laboratory of New Ceramics and Fine Processing, Department of Chemistry and Department of Materials Science and Engineering, Tsinghua University, Beijing 100084, P. R. China, and

[‡]Department of Physics, Peking University, Beijing, 100871, P. R. China

Received September 13, 2009; Revised Manuscript Received November 27, 2009

ABSTRACT: Highly uniform coalescent moniliforme-shape α -Fe₂O₃ straight nanochains built up of single crystal building blocks are synthesized via a facile one-pot solution-phase route at 180 °C using FeCl₃, which have interesting magnetic behaviors based on their unique structure. Surprisingly, an exceptionally high T_M (Morin transition temperature) is observed.

One-dimensional (1D) nanostructures are very appealing, owing to many unique physical and chemical properties based on their high intrinsic anisotropy and surface activity.^{1–4} In recent years, reports on a class of novel 1D oriented architectures built up of small crystals bring us into an expanding field of the self-aggregation of nanomaterials, which opens a possible way to produce some nanochains with fluctuant diameters along their length.^{5,6} Nanochains have a much higher specific ratio area than wire, rod, or belt-shaped nanostructures of equal diameter. Furthermore, it has been demonstrated that the complex coupling interactions between adjacent structure units within nanochains can give rise to extraordinary collective properties.^{6,7} These features are drawing considerable fundamental and practical interest in the field of magnetism. Magnetic nanoparticles have been known to be able to form chains and rings during self-assembly processes depending on interparticle dipole–dipole and other weak interactions; however, to a certain extent, once separated from substrates, those 1D particle trains have difficulty keeping their morphology for a long time.^{8–14} While vermicular coalescent magnetic nanoaggregates are already constructed,^{15,16} up to now, it remains a challenge to prepare uniform 1D straight magnetic nanochains with good stability.

Fe₂O₃ is a sort of low-cost magnetic material of high chemical inactivity. In this communication, a facile one-pot solution-phase route to synthesize highly uniform α -Fe₂O₃ straight-chains without field induction is reported. Our chains have a unique orientational alignment structure and interesting magnetic behaviors. Typically, 1 mM FeCl₃, 3 mM sodium oleate, 6 mL of oleylamine, and 4 mL of oleic acid were dissolved in a mixed solvent of 8 mL of H₂O/4 mL of ethanol/8 mL of *n*-hexane/15 mL of *n*-octane under vigorous magnetic stirring. The obtained yellow mixture was transferred to a Teflon-lined autoclave up to 95% of the capacity. After 5 min of ultrasonic treatment, this system was sealed to heat at 180 °C for 12 h. The final solid product was collected by centrifugation and washed several times with ethanol and *n*-hexane.

X-ray diffraction (XRD) was carried out to determine the crystalline phase characteristics and composition of the as-prepared products. As shown in Figure 1, the series of Bragg reflections in the XRD pattern can be perfectly indexed as the rhombohedral α -Fe₂O₃ [hematite: JCPDS 87-1166, R̄3c (167)]. No other peaks are observed belonging to impurities, such as Fe₃O₄, γ -Fe₂O₃, or other precursor compounds.

Examination by scanning electron microscopy (SEM) and transmission electron microscopy (TEM) reveals that the α -Fe₂O₃ nanostructures are of identical size and morphology

(Figure 2). Such moniliforme-shape straight nanostructures are made up of more than a dozen aggregated polyhedron particle-units with an average diameter of about 19.8 nm, and the uniformity of those building blocks is confirmed by a size distribution histogram (Figure S1 of the Supporting Information). From the SEM images, it is worthy of note that these nanochains have self-assembled along their long axes and then into large-scale 3D stacks on the silicon substrate (Figures 2A and S2). The assemblies were formed via an ordinary solvent evaporation process pathway.

We analyzed the junctions of the building particles in virtue of high-resolution-TEM (HRTEM). Figure 2E is a lattice-resolved HRTEM image taken from the contact area of two contiguous particles. It can be seen that the lattice fringes extend through the two particles without interruption by any visible boundary. The inset corresponds to the associated reversed-phase fast-Fourier-transform (FFT) pattern, which displays only one set of reciprocal spots. These results show the single-crystal nature of the fusion region. The highly oriented characteristic of α -Fe₂O₃ single-crystal attachment is further supported by a selected area electron diffraction (SAED) pattern of two nanochains abutting each other side by side (Figure 2B and C). In addition, we have discovered that some other segments are of low-angle tilting attachment type; that is to say, two neighboring units share one crystal layer, and the joining planes on both sides of each boundary have the same Miller indices (Figure 3).

Characterization of sufficient samples using HRTEM indicates that the building particles are consistently single crystal. Also, the representative HRTEM image reveals clear lattice fringes perpendicular to the long axis of the nanochain with an interplanar distance of ~0.23 nm in Figure 2E, corresponding to the (006) plane of the rhombohedral α -Fe₂O₃. This is in good agreement with the observation from the SAED pattern and indicates that the growth direction of the nanochains is [001], namely the *c*-axis of the crystal. Moreover, it can be noted that the particle-units are truncated hexagonal bipyramids, and through geometric calculation, we estimate that such dodecahedra expose 12 equivalent {113} crystal planes as their surfaces (for details, see Supporting Information).

Based on the above analysis, a possible formation mechanism of our moniliforme-shaped α -Fe₂O₃ nanostructures is schematically illustrated in Scheme 1. As has been widely accepted, controlled synthesis of nanocrystals with homogeneous morphology is feasible by the effects of surfactants selective adhesion, since the organic capping additive molecules can bind tightly to special crystal facets and restrain their development while the others are unlimited.^{17–20} Thus, it is reasonable to understand that, in the first stage, the precursors concentration is high, and

*Corresponding author. Fax: (86) 10 6278 8765. Telephone: (86) 10 62772350. E-mail: ydli@tsinghua.edu.cn.

the metastable polyhedron particles emerge from the solution under a kinetic growth regime and are stabilized by the surfactants oleic acid and oleylamine.^{17,21,22} Atoms in two corners of

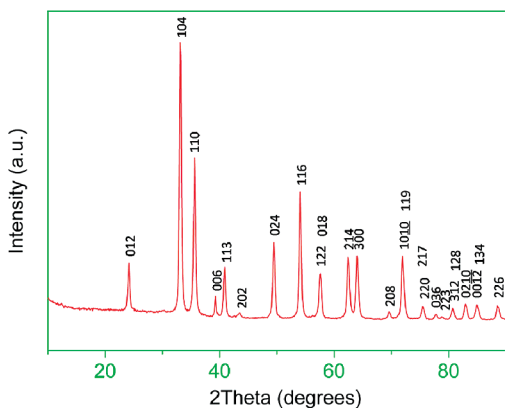


Figure 1. XRD pattern of the as-prepared sample.

every as-formed particle bear comparatively high average free energy because they possess abundant dangling bonds. Then, in the second stage, as the reaction proceeds, the solution concentration gradually decreases, and minimization of the overall surface energy will become the driving force for the evolution of the nanocrystals. Atoms may migrate from the higher surface energy positions to the lower ones, so the cusp parts are dissolved and the primary particles attach to each other in an oriented manner without new facets arising.^{5,23–25} To find supporting experimental evidence, detailed TEM surveys of the samples have been performed. It is expected that individual particles and short segments are detected as intermediates; furthermore, the diameters of these intermediates and the fully developed products are almost the same (Figure 4).^{17,26} In this aggregation-based 1D growth, Brownian motion and interparticle interactions make the close contact of primary nanocrystals possible.²⁴ Single particles and their aggregates are allowed to sway and rotate to achieve the aligned low-energy configuration. Meanwhile, random disturbance of the surrounding medium seems to be a reason for tilting attachment.

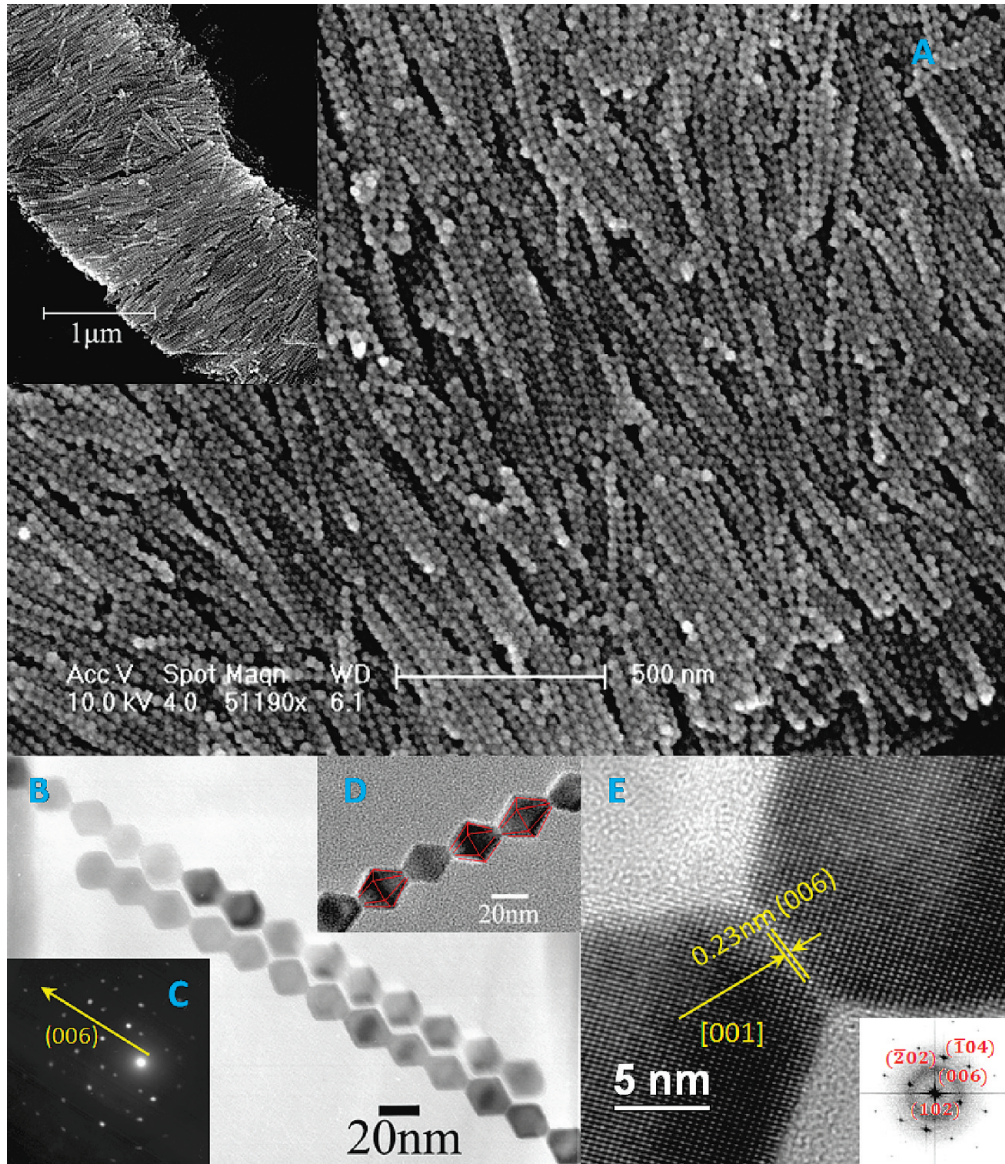


Figure 2. (A) SEM images of the moniliforme-shaped α -Fe₂O₃ nanostructures. (B) TEM image of two nanochains abutting each other side by side. The corresponding electron diffraction pattern is shown in part C). (D) TEM image of the truncated hexagonal bipyramidal particle-units. (E) Lattice-resolved HRTEM image taken from the contact area of two contiguous particles and the associated FFT pattern.

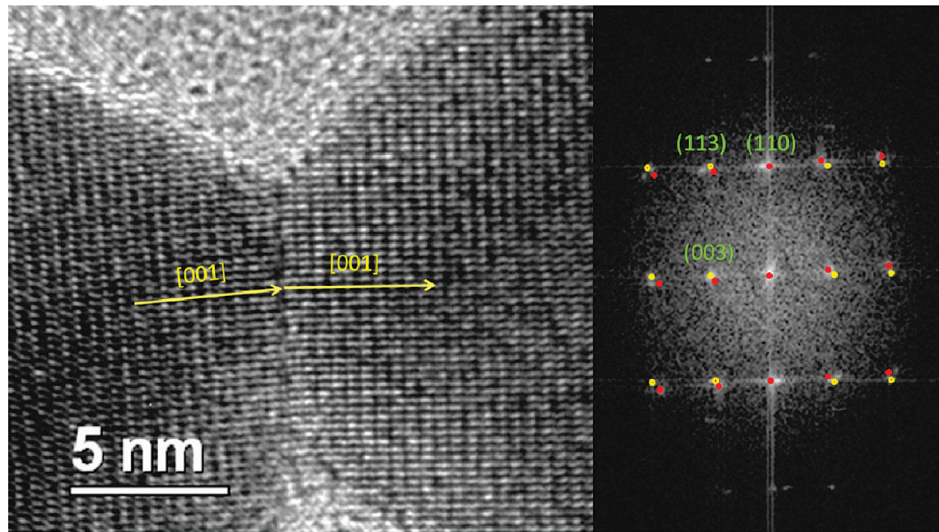


Figure 3. HRTEM image of two neighbor building units which are of low-angle grain boundary attachment type (left). The associated FFT image (right) shows an indexed characteristic double spot-matrix pattern.

Scheme 1. Illustration of the Formation Mechanism of the $\alpha\text{-Fe}_2\text{O}_3$ Nanostructures

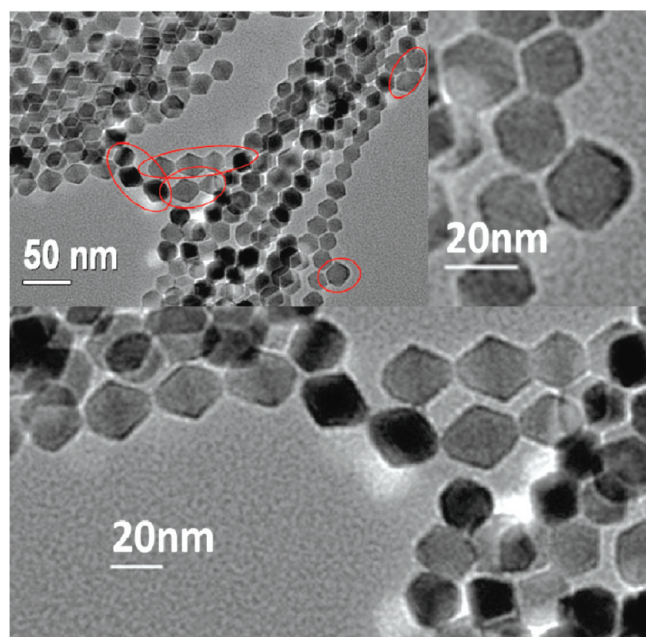
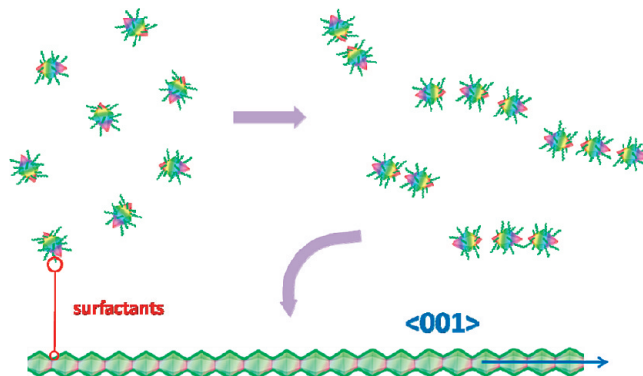


Figure 4. TEM images of individual particles and short segments detected from the sample.

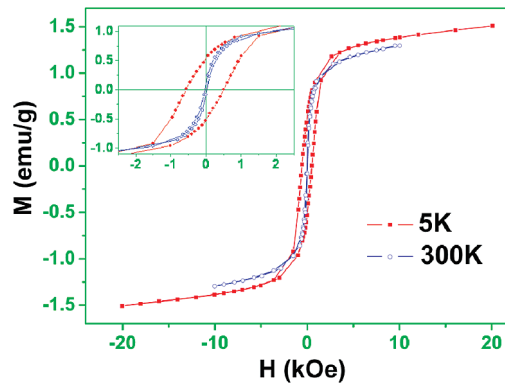


Figure 5. Hysteresis loops of the one-dimensional $\alpha\text{-Fe}_2\text{O}_3$ nanostructures measured at 5 and 300 K.

1D orientation structures give rise to unique magnetic properties due to the shape anisotropy. So we perform magnetization measurements on the powder sample (1.42 mg) of the obtained moniliforme-shape $\alpha\text{-Fe}_2\text{O}_3$ nanostructures with a superconducting quantum interference device (SQUID) magnetometer, including $M-H$ measurements at $T = 5$ and 300 K and $M-T$ measurements from $T = 5$ to 360 K. The $M-H$ magnetization curves are shown in Figure 5. At 300 K, there is nearly no hysteresis. At low temperature ($T = 5$ K), however, the $M-H$ curve displays a loop with a coercivity of about 540 Oe and a remnant magnetization of about 0.53 emu/g. The coercivity is markedly enhanced from those of $\alpha\text{-Fe}_2\text{O}_3$ nanoparticles and nanorods at low temperature.^{27,28} The large remnant magnetization along with the much enhanced coercivity may partly be associated with the strong exchange coupling between building units of the $\alpha\text{-Fe}_2\text{O}_3$ chains and the orientational alignment of the nanoarchitectures, leading to the significant shape anisotropy. Figure 6 shows the field-cooled (FC) and zero-field-cooled (ZFC) $M-T$ data. As clearly revealed by the separation of the FC and ZFC curves, the blocking temperature of the $\alpha\text{-Fe}_2\text{O}_3$ nanochains exceeds the highest temperature of measurement, 360 K. This indicates the presence of a large magnetic anisotropy energy barrier associated with the 1D structure. Otherwise, one would expect to observe a superparamagnetic behavior with a much lower blocking temperature for disconnecting nanoparticles.

It has been known that the bulk hematite is antiferromagnetic (AFM) below a first-order magnetic transition temperature T_M

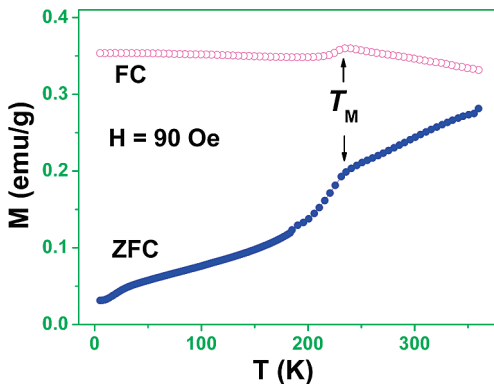


Figure 6. ZFC and FC magnetizations of the obtained α - Fe_2O_3 nanostructures (measurements were performed in an applied field of 90 Oe).

(the Morin transition temperature, about 260 K) and is in a weak ferromagnetic (FM) state between T_M and T_N (Néel temperature, about 950 K).^{29–32} But in the nanoscaled regime, T_M usually decreases with the grain size as a result of the crystallinity or surface properties.³³ For instance, $T_M \sim 200$ K was observed for 40 nm and ~ 186 K for 36 nm hematite nanoparticles.³⁴ It even reduces down to below 5 K or completely disappears.^{31,35} The unideal crystallinity would usually suppress the reorientation transition of the moments at the two sublattice sites, changing from a canted alignment within the $a-b$ basal plane (weak FM state) to an antiparallel alignment along the c -axis (AFM state). With our as-synthesized α - Fe_2O_3 nanopowder, however, T_M occurs at about 237 K, as revealed by the sharp feature in the FC and ZFC curves (Figure 6). It is only slightly reduced from the bulk value, indicating a well-crystallized condition for the nanochains, as already shown by the HRTEM and TEM images in Figures 3 and 4. The novel structure of the AFM α - Fe_2O_3 chains is interesting for a deeper investigation toward a more comprehensive understanding of the related magnetic properties.

In summary, highly uniform moniliforme-shape α - Fe_2O_3 straight-chains were synthesized under one-pot hydrothermal treatment at 180 °C. Such one-dimensional coalescent architectures were built up of single crystal building blocks with an average diameter of 19.8 nm. The interesting orientational alignment of building blocks ensures the straightness of the α - Fe_2O_3 architectures, whose coercivity of about 540 Oe at 5 K and a large remnant magnetization due to the unique structure are determined by $M-H$ measurements. The Morin transition, ~ 237 K, is only slightly reduced from the bulk value, ~ 260 K, and it is much higher than that reported for nanoparticles of the same material with the diameter in the range of 20 nm or so on account of the good crystallinity of the sample. This kind of nanochains may serve as an ideal model for magnetic study of nanoscale anti-ferromagnetic materials or be used as magnetic-drive probes.

Acknowledgment. This work was supported by NSFC (20921001, 90606006, 10874006) and the State Key Project of Fundamental Research for Nanoscience and Nanotechnology (2006CB932300).

Supporting Information Available: Reagents and characterization details, some more figures, and additional geometrical

http://pubs.acs.org 上获得。

References

- Wang, Z. *Adv. Mater.* **2003**, *15*, 432–436.
- Baca, A. J.; Ahn, J. H.; Sun, Y.; Meitl, M. A.; Menard, E.; Kim, H. S.; Choi, W. M.; Kim, D. H.; Huang, Y.; Rogers, J. A. *Angew. Chem., Int. Ed.* **2008**, *47*, 5524–5542.
- Xia, Y. N.; Yang, P. D.; Sun, Y. G.; Wu, Y. Y.; Mayers, B.; Gates, B.; Yin, Y. D.; Kim, F.; Yan, Y. Q. *Adv. Mater.* **2003**, *15*, 353–389.
- Kuchibhatla, S. V.; Karakoti, A. S.; Bera, D.; Seal, S. *Prog. Mater. Sci.* **2007**, *52*, 699–913.
- Penn, R. L.; Banfield, J. F. *Geochim. Cosmochim. Acta* **1999**, *63*, 1549–1557.
- Tang, Z. Y.; Kotov, N. A. *Adv. Mater.* **2005**, *17*, 951–962.
- Nie, Z. H.; Fava, D.; Kumacheva, E.; Zou, S.; Walker, G. C.; Rubinstein, M. *Nat. Mater.* **2007**, *6*, 609–614.
- Butter, K.; Bomans, P.; Frederik, P. M.; Vroege, G. J.; Philipse, A. P. *Nat. Mater.* **2003**, *2*, 88–91.
- Hu, M. J.; Lu, Y.; Zhang, S.; Guo, S. R.; Lin, B.; Zhang, M.; Yu, S. H. *J. Am. Chem. Soc.* **2008**, *130*, 11606–11607.
- Tripp, S. L.; Pusztay, S. V.; Ribbe, A. E.; Wei, A. *J. Am. Chem. Soc.* **2002**, *124*, 7914–7915.
- Klokkenburg, M.; Vonk, C.; Claesson, E. M.; Meeldijk, J. D.; Erne, B. H.; Philipse, A. P. *J. Am. Chem. Soc.* **2004**, *126*, 16706–16707.
- Korth, B. D.; Keng, P.; Shim, I.; Bowles, S. E.; Tang, C.; Kowalewski, T.; Nebesny, K. W.; Pyun, J. *J. Am. Chem. Soc.* **2006**, *128*, 6562–6563.
- Lalattonne, Y.; Richardi, J.; Pilani, M. P. *Nat. Mater.* **2004**, *3*, 121–125.
- Salgueirino-Maceira, V.; Correa-Duarte, M. A.; Hucht, A.; Farle, M. *J. Magn. Magn. Mater.* **2006**, *303*, 163–166.
- Liu, C. M.; Guo, L.; Wang, R. M.; Deng, Y.; Xu, H. B.; Yang, S. H. *Chem. Commun.* **2004**, 2726–2727.
- Zhou, W.; Zheng, K.; He, L.; Wang, R. M.; Guo, L.; Chen, C. P.; Han, X.; Zhang, Z. *Nano Lett.* **2008**, *8*, 1147–1152.
- Yin, Y.; Alivisatos, A. P. *Nature* **2005**, *437*, 664–670.
- Lee, S. M.; Cho, S. N.; Cheon, J. *Adv. Mater.* **2003**, *15*, 441–444.
- Viswanatha, R.; Battaglia, D. M.; Curtis, M. E.; Mishima, T. D.; Johnson, M. B.; Peng, X. *Nano Res.* **2008**, *1*, 138–144.
- Jun, Y. W.; Casula, M. F.; Sim, J. H.; Kim, S. Y.; Cheon, J.; Alivisatos, A. P. *J. Am. Chem. Soc.* **2003**, *125*, 15981–15985.
- Peng, Z. A.; Peng, X. G. *J. Am. Chem. Soc.* **2001**, *123*, 1389–1395.
- Peng, Z. A.; Peng, X. G. *J. Am. Chem. Soc.* **2002**, *124*, 3343–3353.
- Penn, R. L.; Banfield, J. F. *Science* **1998**, *281*, 969–971.
- Banfield, J. F.; Welch, S. A.; Zhang, H. Z.; Ebert, T. T.; Penn, R. L. *Science* **2000**, *289*, 751–754.
- Alivisatos, A. P. *Science* **2000**, *289*, 736–737.
- Tang, Z. Y.; Kotov, N. A.; Giersig, M. *Science* **2002**, *297*, 237–240.
- Tang, B.; Wang, G. L.; Zhuo, L. H.; Ge, J. C.; Cui, L. J. *Inorg. Chem.* **2006**, *45*, 5196–5200.
- Liu, L.; Kou, H. Z.; Mo, W. L.; Liu, H. J.; Wang, Y. Q. *J. Phys. Chem. B* **2006**, *110*, 15218–15223.
- Morin, F. J. *Phys. Rev.* **1950**, *78*, 819–820.
- Shull, C. G.; Strauser, W. A.; Wollan, E. O. *Phys. Rev.* **1951**, *83*, 333–345.
- Amin, N.; Arajs, S. *Phys. Rev. B* **1987**, *35*, 4810–4811.
- Besser, P. J.; Morrish, A. H.; Searle, C. W. *Phys. Rev.* **1967**, *153*, 632–640.
- Schroere, D.; Nininger, R. C. *Phys. Rev. Lett.* **1967**, *19*, 632–634.
- Zysler, R. D.; Fiorani, D.; Testa, A. M.; Suber, L.; Agostinelli, E.; Godinho, M. *Phys. Rev. B* **2003**, *68*, 212408.
- Jiao, F.; Harrison, A.; Jumas, J. C.; Chadwick, A. V.; Kockelmann, W.; Bruce, P. G. *J. Am. Chem. Soc.* **2006**, *128*, 5468–5474.